



Design and analysis of broadband guided-mode resonant reflectors with coated triangular and trapezoidal profiles in TE polarization

GUOHUA XING,^{1,2} SHANWEN ZHANG,^{1,3,5} XIAOTAO MI,¹  AND RONGJUN ZHANG^{4,6}

¹National Engineering Research Center for Diffraction Gratings Manufacturing and Application, Changchun Institute of Optics and Fine Mechanics and Physics, Chinese Academy of Sciences, Changchun, Jilin 130033, China

²University of Chinese Academy of Sciences, Beijing 101408, China

³Engineering Research Center of Mechanical Testing Technology and Equipment, Ministry of Education, Chongqing Key Laboratory of Time-Grating Sensing and Advanced Testing Technology, Chongqing University of Technology, Chongqing 400054, China

⁴Department of Optical Science and Engineering, Fudan University, Shanghai 200433, China

⁵zhshwen007@163.com

⁶rjzhang@fudan.edu.cn

Abstract: A low-refractive-index grating layer with symmetrical triangular/trapezoidal grooves covered with a high-refractive-index Si layer is used to design a broadband guided-mode resonant reflector. Software Rsoft is used to simulate the reflection and transmission spectra as well as the internal electric field distribution at the resonant wavelength. It is discovered that the interaction between resonant modes promotes the formation of a wideband spectrum. The reflector has been proven to provide wideband ($\Delta\lambda > 450$ nm) and high reflectivity ($R > 98.4\%$) spectra over a wide range of base angles from 44° to 72° , and the maximum high reflectivity ($R > 99\%$) spectral range in transverse electric polarization is 458 nm, spanning 1422 to 1880 nm. The results not only demonstrate excellent tolerance to the base angle and grating depth but also provide more possibilities for the design of broadband reflectors.

© 2021 Optical Society of America under the terms of the [OSA Open Access Publishing Agreement](#)

1. Introduction

Most optical mirrors with high reflectivity have been extensively investigated in the fields of imaging, telecommunications, and sensors. Traditional metal mirrors have low reflectivity owing to the limitations of material absorption loss. Dielectric stacking mirrors require 10–100 quarter- and/or half-wave layers to achieve high reflectivity, and the layer thickness and refractive index are strictly controlled. To improve the reflectivity and reduce the number of layers, photonic crystals, subwavelength gratings, and metamaterial structures [1–5] have been developed to replace metal reflectors and dielectric stack reflectors. In particular, the periodic subwavelength grating reflector, also known as the guided-mode resonance (GMR) reflector, can induce the GMR effect and yield high reflectivity through a few layers with optimal parameters [2,6–9]. In addition, a reflectivity close to unity in a broadband range can be achieved by the excitation and interaction of multiple guided-mode resonances. These facts indicate that GMR reflectors offer the advantages of simple structure and ultra-high diffraction efficiency; hence, they are used extensively in lasers, wave plates, detectors, and couplers [10–16].

Transverse magnetic (TM) and transverse electric (TE) grating reflectors based on GMR effects have been extensively investigated previously. The polarization-dependent boundary condition of GMR grating determines the difference of the distribution of resonant modes in TE and TM, which leads to the differences in optimal parameters and spectrum performance [17–18]. The modal curves in the TM case present sufficient curvature and spectral proximity [17], and

are more capable of providing broadband reflection function than TE case, so the research of broadband GMR reflectors is mainly focused on TM polarization. For example, Chang–Hasnain et al. designed a high-contrast grating (HCG) structure [9] that yielded high reflectivity ($R > 99\%$) over a wide spectral range of approximately 520 nm in TM case, and the large refractive index difference between materials contributed to the generation of a broadband spectrum. By contrast, Magnusson et al. proposed zero-contrast grating (ZCG) reflectors, in which the refractive index of the grating layer matched the homogeneous layer, and the bandwidth was reported to be ~ 700 nm [8]. Subsequently, based on the two structures above, researchers designed many ultra-wideband grating reflectors with different profiles, periods, and materials in TM polarization, such as multi-period [19], three-layer [20], hybrid [21], double-layer subwavelength [22], and symmetric triangle/trapezoid grating reflectors [23–24]. For the TE polarization, a multi-subpart profile grating reflector with four subparts was proposed to demonstrate a bandwidth of 630 nm [25]. However, the bandwidths of the simpler two-subpart periodic ZCG [26] and HCG [2] were narrower, i.e., 380 and 125 nm, respectively. Herein, we propose a new GMR grating structure for TE polarization to ameliorate this condition.

GMR reflectors with triangular/trapezoidal profiles comprising a low-refractive-index grating layer and a high-refractive-index film layer are proposed herein. We point out that although they are all broadband reflectors with triangular or trapezoidal groove, the waveguide layer structure and the polarization performance presented here are completely different from those in [24]. We simulated the mode evolution corresponding to wideband reflection spectra formation and discovered that the number and location of resonance modes changed with the structural parameters, thereby realizing reflection bandwidth tuning. It has been proven that the structure shows not only a broadband high reflectivity spectrum in a wide range of base angles under TE polarization, but also a better tolerance to the device parameters. To the best of our knowledge, for the simpler two-subpart GMR reflectors reported for TE polarization, our design offers the best performance in terms of bandwidth and reflectivity.

2. Device structure

The proposed GMR reflectors are shown in Fig. 1. The low-refractive-index SiO_2 layer ($n_s = 1.48$) serves as a substrate and a symmetrical triangular and trapezoidal groove grating with a period of Λ , base angles α and β , and depth of groove d_g . The yellow high-refractive-index Si material ($n = 3.48$) covered above acts as a waveguide layer with a height of d_L , with a gradient distribution of equivalent refractive index.

For the rectangular groove broadband reflectors with fixed index, the structural difference between TE [26] and TM [8] polarization is reflected in the parameters: it has smaller period and larger thickness for TM reflectors [18]. However, the structural difference of triangular/trapezoidal groove broadband reflectors with gradient index is reflected not only in the parameters, but only in the distribution of equivalent refractive index along the z -direction. The effective refractive for each layer of broadband triangular grooves grating with same parameters in TE and TM polarization using effective medium theory are shown in Fig. 2. The TM reflectors in [24] is topped with a triangular groove grating with a gradient equivalent refractive index from n to n_c , but it shows different concavity than the top grating of TE reflectors designed here due to the difference of the equivalent refractive index as expressed in Eq. (1) and (2). On this basis, TE reflectors additionally introduce a low refractive index triangular groove grating at the bottom of the structure, with an effective refractive index gradient opposite to the top grating, from n_s to n . Therefore, the TE reflectors can be equivalent to an inverted double grating structure along the z -direction.

$$n_{eff,TE}^2 = F n_H^2 + (1 - F) n_L^2 \quad (1)$$

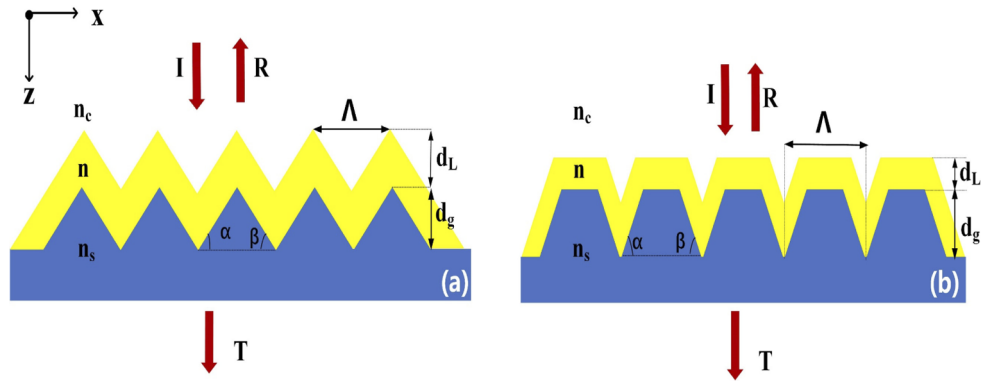


Fig. 1. Schematic view of broadband GMR reflectors with coated (a) triangular and (b) trapezoidal profile. In the structure, high refractive index film layer of Si ($n = 3.48$) forms conformal coverage on low refractive index grating layer of SiO_2 ($n_s = 1.48$). Light of TE polarization is incident on structure normally from air ($n_c = 1$).

$$\frac{1}{n_{eff, TM}^2} = \frac{F}{n_H^2} + \frac{(1-F)}{n_L^2} \quad (2)$$

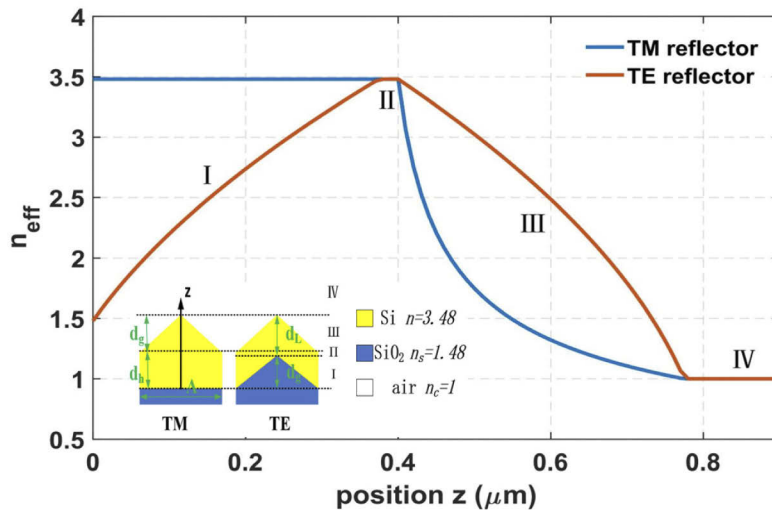


Fig. 2. The effective refractive index for each layer of broadband triangular grooves grating reflectors in TE and TM polarization using effective medium theory. The inset displays the structures of TE and TM reflectors with same parameters. Parameters: $\Lambda = 0.75 \mu\text{m}$, $d_g = 0.375 \mu\text{m}$, $d_h = d_L = 0.4 \mu\text{m}$.

Nano-imprinting fabrication method is considered to implementing the coated triangular and trapezoidal profiles grating which is technically easier than mechanical ruling considered to fabricate the grating in [24].

3. Evaluation of resonant modes

“DiffractMOD” in RSoft was used to obtain the optimal parameters and field distribution of the GMR grating. DiffractMOD is a tool for the design of diffractive optical structures, in which the

rigorous coupled-wave analysis (RCWA) method [27] is used to simulate the electromagnetic wave diffraction of periodic structures. The incident plane wave can have an arbitrary direction and polarization, and all types of simulation results can be output, including diffraction efficiency, near field, and far field results.

We remark that the period Λ , base angle α , and groove thickness d_g of the reflector with a triangular profile satisfy $d_g = \Lambda \tan(\alpha/2)$. Moreover, the grating groove will evolve from a triangle to a trapezoid with a decrease in the thickness of the grating layer d_g , while maintaining a constant base angle. For simplification, we fixed the thickness of the high-refractive-index film to 400 nm, and the two base angles of the triangular and trapezoidal grooves were symmetrical.

Figures 3(a)–(h) present the transmission contour maps $T_0(\lambda, d_g)$ on a logarithmic scale with the wavelength and groove depth for the base angles of 20°, 40°, 44°, 45°, 46°, 60°, 72°, and 75°, respectively. In these contour maps, the red region represents high transmission, and the yellow region represents high reflectivity caused by the GMR. As shown in Fig. 3(a), at $\alpha = 20^\circ$, three vertically distributed modes were observed, i.e., at 1.2, 1.6, and 2.4 μm , and their positions were almost independent of the grating thickness. With an increase in the base angle, a new mode appeared, and the modes at both ends shifted to the middle. However, the modes distributed at different grating depths shifted at different speeds, resulting in the bending of the modes, as shown in Fig. 3(b). When the three modes shifted by an appropriate distance, they interacted with each other to produce a high reflection spectrum ($R > 99\%$) from 1430 to 1882 nm at the maximum grating layer thickness, which corresponds to a broadband reflector with a triangular groove, as shown in Fig. 3(c). When $\alpha = 45^\circ$, as shown in Fig. 3(d), the two modes on the right region combined to form a mixed mode, and when $\alpha = 46^\circ$, as shown in Fig. 3(e), the mixed mode bent and shifted downward, forming a broadband spectrum at $d_g = 0.326 \mu\text{m}$. Subsequently, the mode shown on the left side of Fig. 3(f) bent in the long-wavelength direction under the attraction of the mixed mode, and the distance between the two modes decreased gradually as the base angle increased. At $\alpha = 72^\circ$ in Fig. 3(g), the two modes shifted by the least distance, resulting in a strong interaction between them; hence, an ultra-high reflectivity ($R > 99.9\%$) can be achieved in a broadband range (308 nm). As illustrated in Fig. 3(h), the resonant modes rearranged and combined to form new mode distributions, and the two new modes repel each other, thereby weakening the interaction between them; consequently, the characteristics of wideband and high reflection of the GMR reflectors will not be maintained.

The GMR reflectors with triangular or trapezoidal profiles can yield high reflectivity over a wide bandwidth, and the characteristics are jointly contributed by the three resonant modes. The strong interaction between the close resonant modes ensures high reflectivity but reduces the bandwidth, whereas the weaker interaction between the distant resonant modes yields a wider bandwidth but a lower reflectivity. The relative distance between the resonant modes can be controlled by the structural parameters, such as the base angle and grating thickness, to tune the bandwidth and reflectivity. In particular, the structure parameters corresponding to the broadband reflection are not unique, but can be realized for any base angles between 44° and 72°, as shown in the yellow area in Fig. 3.

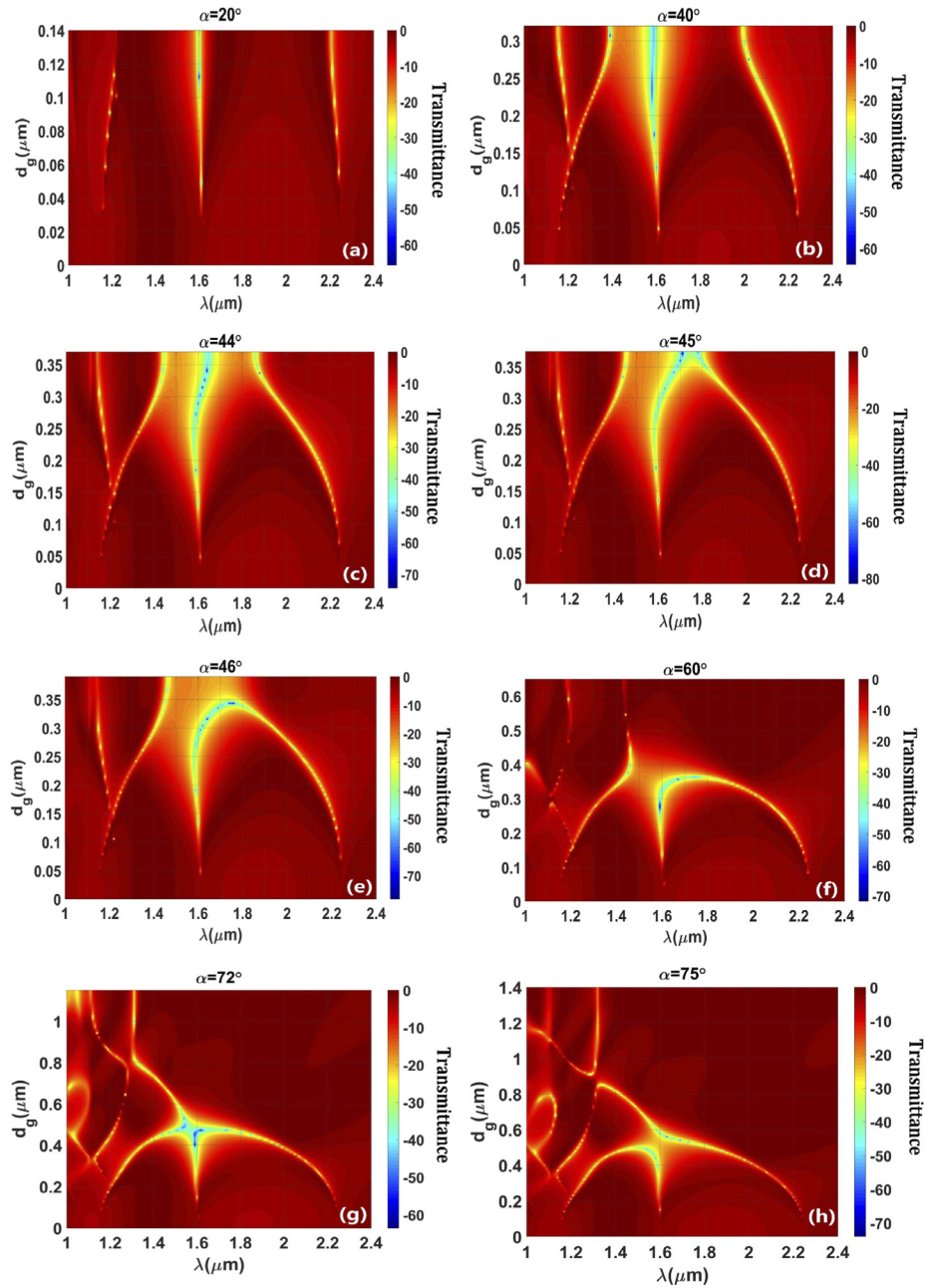


Fig. 3. Transmittance map $T_0(\lambda, d_g)$ on logarithmic scale vs. wavelength and thickness of low refractive index grating layer with triangular and trapezoidal profiles for $\Lambda = 750$ nm, $d_L = 400$ nm, with eight different base angles. (a) $\alpha = 20^\circ$; (b) $\alpha = 40^\circ$; (c) $\alpha = 44^\circ$; (d) $\alpha = 45^\circ$; (e) $\alpha = 46^\circ$; (f) $\alpha = 60^\circ$; (g) $\alpha = 72^\circ$; (h) $\alpha = 75^\circ$.

4. Result

The GMR reflector can realize wideband reflection over a wide range of base angles. To highlight this point, we simulated the reflection and transmission spectra at different base angles, and only three representative values were selected for simplification.

Figure 4 shows the optimized reflection and transmission spectra on the linear and logarithmic scales of the GMR reflectors with the coated trapezoidal groove at $\alpha = 46^\circ$, 60° , and 72° . As shown in Fig. 4(a), the GMR reflectors with optimized parameters $\alpha = 46^\circ$, and $d_g = 326$ nm exhibited high reflectivity ($R > 99\%$) over a 458 nm bandwidth in the 1422–1880 nm range. In the band range, three transmission dips were observed, each of which represents a GMR, at $\lambda = 1435$, 1663, and 1857 nm. The spectral bandwidths demonstrated exceeded previously reported results for simpler two-part periodic reflectors operating in TE polarization. This mainly arise from the fact that the incident light with different wavelengths can be effectively coupled into the waveguide layer at the cross-sectional area of different duty cycle. For the GMR reflector with optimized parameters $\alpha = 60^\circ$, and $d_g = 359$ nm, as shown in Fig. 4(b), a high reflectivity ($R > 98.4\%$) from 1416 to 1870 nm spanning a 454 nm range was obtained. Similarly, three guided-mode resonances that occur at $\lambda = 1430$ nm, 1678 nm, and 1824 nm, and the distance between two modes on the short wavelength direction induces a decrease in local reflectivity at $\lambda = 1491$ nm. As shown in the dotted curve in Fig. 4(c), when the base angle increased to 72° and the grating thickness increased to 475 nm, a strong interaction occurred between the resonant modes, resulting in ultra-high reflectivity ($R > 99.9\%$) in a wide band range (308 nm) from 1493 to 1747 nm. Moreover, when the grating depth was 448 nm, a high reflectivity ($R > 98.4\%$) bandwidth of 464 nm from 1415 to 1879 nm was indicated, as represented by the solid curve in Fig. 4(c).

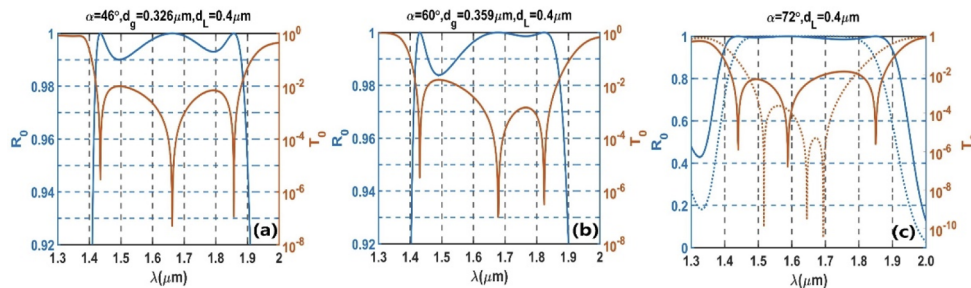


Fig. 4. Linear reflectance and logarithmic transmittance spectra of GMR reflectors with coated trapezoidal profiles at (a) $\Lambda = 750$ nm, $\alpha = \beta = 46^\circ$, $d_L = 400$ nm, and $d_g = 326$ nm, (b) $\Lambda = 750$ nm, $\alpha = \beta = 60^\circ$, $d_g = 359$ nm, and $d_L = 400$ nm, (c) $\Lambda = 750$ nm, $\alpha = \beta = 72^\circ$, $d_L = 400$ nm, $d_g = 448$ nm, and $d_g = 475$ nm.

In addition, we noted that the broadband GMR grating reflector designed here only work in TE polarization, with several independent high reflection peaks in other polarization instead. Conversely, the broadband reflectors proposed in [24] only work in TM polarization, and present a few independent narrow reflection peaks under TE polarization.

The electric field amplitude distribution inside and around the grating at the resonant wavelengths is illustrated in Fig. 5. At the positions of the short resonant wavelength corresponding to Figs. 5(a), (d), and (g), the field was distributed in both the high- and low-refractive-index grating layers and was gradually pushed to the coated layer as the base angle increased. In Figs. 5(b), (e), and (h), for $\lambda = 1.663$, 1.678, and 1.588 μm , the field was pushed to the coated layer and the boundary between the high- and low-refractive-index layers, showing the characteristics of TE_1 . For the long wavelength shown in Figs. 5(c), (f), and (i), the field was only distributed at the bottom of the high-refractive-index layer.

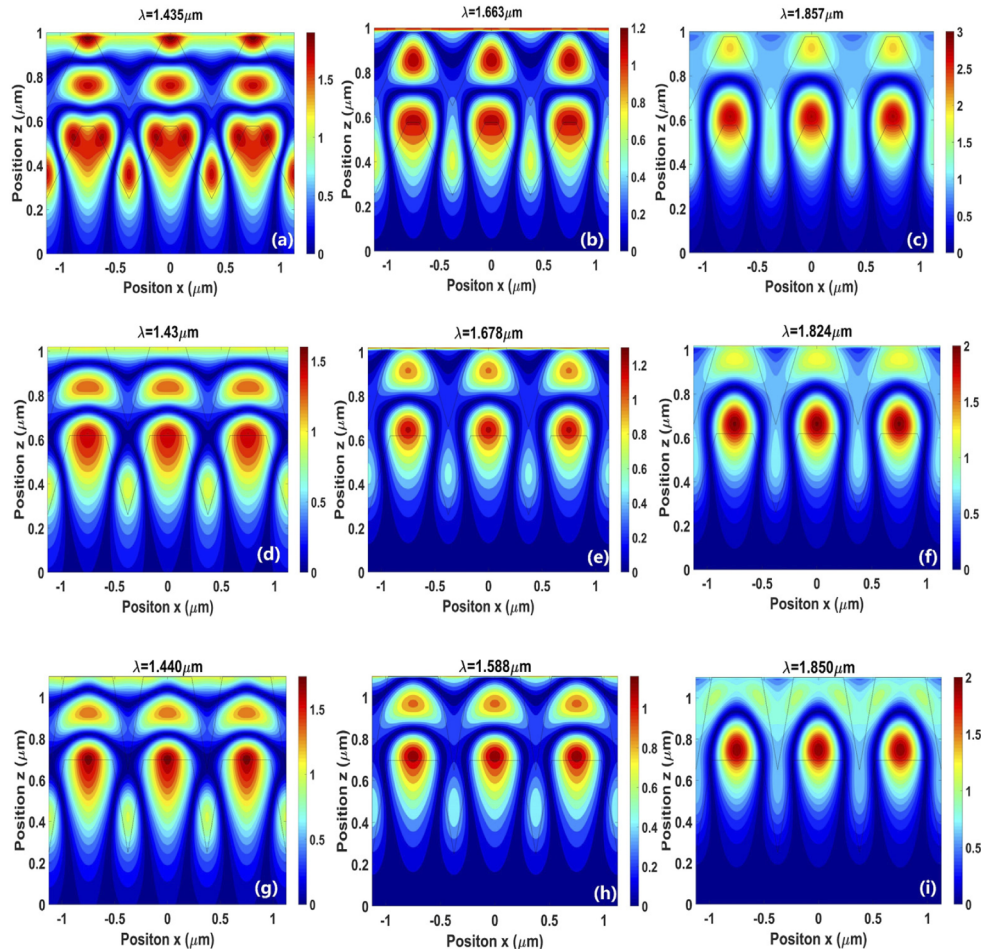


Fig. 5. Internal electric field distributions in and around grating structure with coated trapezoidal groove at resonance wavelengths under different device parameters. (a)-(c) Structure with $\alpha = 46^\circ$ and $d_g = 326$ nm at resonance wavelengths $\lambda = 1.435$, 1.663 , and 1.857 μm , respectively. (d)-(f) Grating structure for $\alpha = 60^\circ$ and $d_g = 359$ nm at resonance wavelengths $\lambda = 1.43$, 1.678 , and 1.824 μm , respectively. (g)-(i) Grating structure for $\alpha = 72^\circ$ and $d_g = 453$ nm at resonance wavelengths $\lambda = 1.440$, 1.588 , and 1.850 μm , respectively.

5. Analysis

5.1. Effect of grating thickness

The high reflectivity bandwidth of the reflectors was affected by the grating thickness because the position of the GMRs varied with d_g . Figure 6(a) presents a zero-order reflectance contour map $R_0(\lambda, d_g)$ depicting the wavelength and grating depth for $\alpha = 46^\circ$, and $d_L = 400$ nm. When the grating depth d_g was less than 320 nm, the reflection spectrum was partitioned into three regions and did not exhibit the characteristics of broadband reflection. As the grating depth increased, the resonant modes at both ends shifted closer to the middle gradually, and they interacted with each other to form a widest high reflection spectrum at $d_g = 326$ nm. Furthermore, when the grating thickness d_g was larger than 326 nm, the three modes continued to approach each other under the attraction force; therefore, the reflection bandwidth decreased as the grating thickness increased.

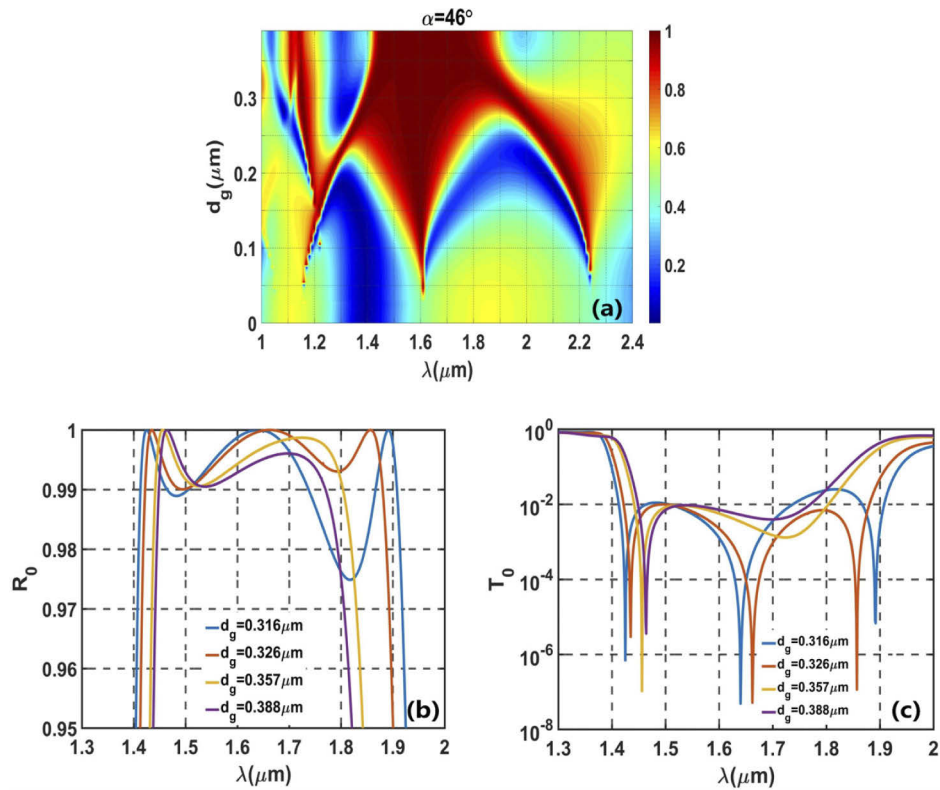


Fig. 6. (a) Contour map of zero-order reflectance of wavelength and grating layer depth for $\Lambda = 750$ nm, $\alpha = 46^\circ$, and $d_L = 400$ nm; (b) zero-order reflectance (linear scale) and (c) transmittance (log scale) spectra for $d_g = 316, 326, 357,$ and 388 nm.

To clarify the tolerance to grating depth, Figs. 6(b) and (c) present the linear reflection and logarithmic transmission spectra of the reflector under different grating depths. The reflection bandwidths are listed in Table 1 corresponding to reflectivity greater than 99% and 97%, separately. For $d_g = 316$ nm, as represented by the blue curve, the two resonant modes on the right were extremely distant from each other, causing the reflectivity to decrease to approximately 97% at $\lambda = 1817$ nm; in this case, $R > 97\%$ can be achieved in the 510 nm band range from 1408 to 1918 nm. The widest reflection bandwidth corresponding to $d_g = 326$ nm was 458 nm; additionally, as the grating thickness increased to 388 nm in the purple curve, the proximity of the three resonant modes resulted in a narrowing of the reflectivity bandwidth, yielding $R_0 > 99\%$

across a 321 nm bandwidth. Therefore, the reflectors exhibited high reflectivity ($R > 99\%$) over a wide range of grating depths ($\Delta d_g = 62$ nm), and its reflection bandwidth decreased gradually from 458 to 321 nm as the grating thickness increased.

Table 1. Bandwidth of GMR Reflector Under Different Grating Depths

R_0	$\alpha = 46^\circ, d_L = 400$ nm			
	$d_g = 316$ nm	$d_g = 326$ nm	$d_g = 357$ nm	$d_g = 388$ nm
$R_0 > 99\%$	$\Delta\lambda = 231$ nm	$\Delta\lambda = 458$ nm	$\Delta\lambda = 361$ nm	$\Delta\lambda = 321$ nm
$R_0 > 97\%$	$\Delta\lambda = 510$ nm	$\Delta\lambda = 476$ nm	$\Delta\lambda = 394$ nm	$\Delta\lambda = 363$ nm

5.2. Effect of base angle

Figure 7(a) shows the reflectance contour map $R_0(\lambda, \alpha)$ for the base angle and wavelength for $d_g = 326$ nm, and $d_L = 400$ nm; as shown, the reflection bandwidth is associated closely with the base angle. For better clarity, the reflection spectra on a linear scale and the transmission spectra on a logarithmic scale at four base angles are presented in Figs. 7(b) and (c), respectively. Compared with the case of $\alpha = 46^\circ$, the two resonant modes on the right were opposite each other when $\alpha = 44^\circ$, as presented by the blue curve, which resulted in a wider bandwidth but a decrease in the local reflectivity at $\lambda = 1882$ nm. However, when $\alpha = 48^\circ$, corresponding to the yellow curve, the two resonant modes on the right shifted toward each other, thereby ensuring high reflectivity but a narrower bandwidth. The bandwidth corresponding to reflectivity greater than 99%, 98%, and 96% are presented in Table 2. When the grating structure was asymmetric, as shown by the purple curve, i.e., $\alpha \neq \beta$, the characteristics of broadband reflection was preserved. In this case, the reflectivity was greater than 98% from 1418 to 1901 nm (spanning a 483 nm band range), which effectively reduced the effect of the manufacturing error of the grating base angle on the reflection spectrum.

Table 2. Bandwidth of GMR Reflector Under Different Base Angles

R_0	$d_g = 326$ nm, $d_L = 400$ nm			
	$\alpha = \beta = 44^\circ$	$\alpha = \beta = 46^\circ$	$\alpha = \beta = 48^\circ$	$\alpha = 46^\circ, \beta = 44^\circ$
$R_0 > 99\%$	$\Delta\lambda = 304$ nm	$\Delta\lambda = 458$ nm	$\Delta\lambda = 337$ nm	$\Delta\lambda = 333$ nm
$R_0 > 98\%$	$\Delta\lambda = 344$ nm	$\Delta\lambda = 468$ nm	$\Delta\lambda = 457$ nm	$\Delta\lambda = 483$ nm
$R_0 > 96\%$	$\Delta\lambda = 513$ nm	$\Delta\lambda = 481$ nm	$\Delta\lambda = 471$ nm	$\Delta\lambda = 496$ nm

5.3. Effect of coated layer thickness

The reflection contour map $R_0(\lambda, d_L)$ shown in Fig. 8(a) directly reflects the variations in reflectivity and bandwidth with the coated layer depth and wavelength under $d_g = 326$ nm, and $\alpha = 46^\circ$. Figures 8(b) and (c) show the linear reflection and logarithmic transmission spectra, respectively, at $d_L = 390, 400,$ and 410 nm. It was clear that as d_L increased, the reflection spectrum shifted gradually toward the long-wavelength direction in Fig. 8(b). Similarly, as shown in Fig. 8(c), the left resonant modes shifted close to each other gradually, resulting in an increase in the local reflectivity at a short wavelength, whereas the resonant modes on the right repelled from each other gradually, resulting in a decrease in the local reflectivity at a long wavelength. Table 3 shows that when the thickness of the coated layer changed by 10 nm, the variation range of the high reflectivity bandwidth was approximately 156 or 182 nm; therefore, the reflectivity spectra were sensitive to the film depths compared with the base angle and grating thickness.

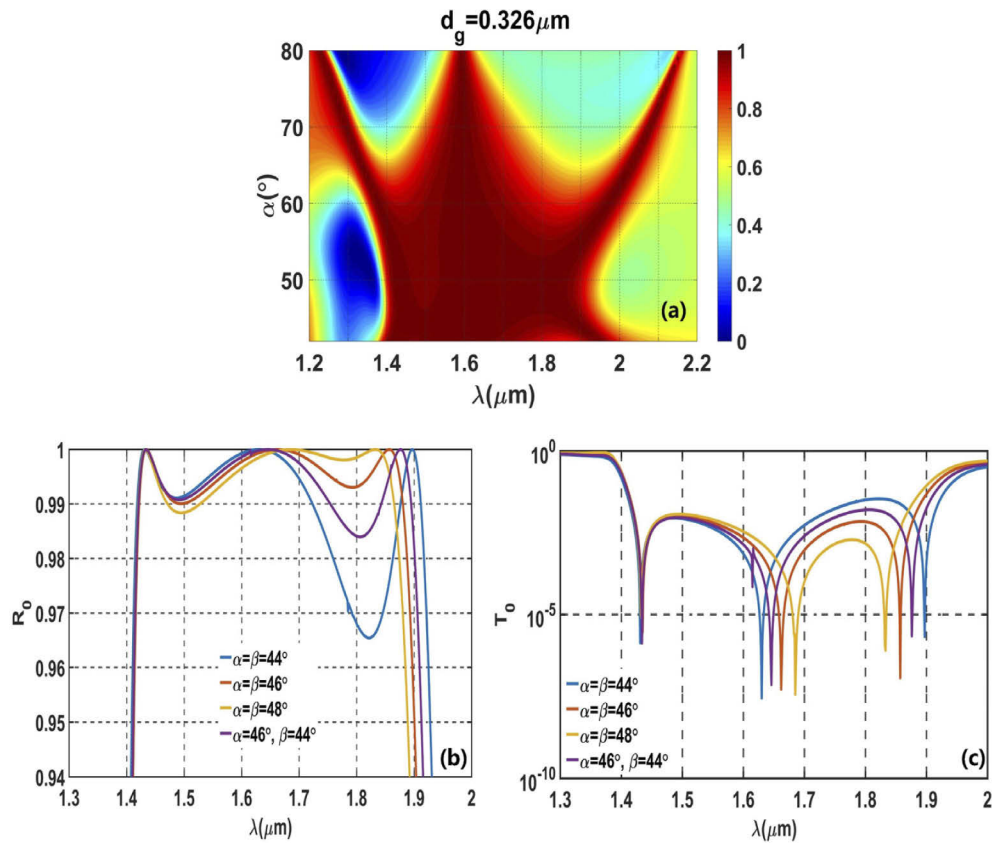


Fig. 7. (a) Contour map of zero-order reflectance of wavelength and base angle for $\Lambda = 750 \text{ nm}$, $d_g = 326 \text{ nm}$, and $d_L = 400 \text{ nm}$; (b) zero-order reflectance (linear scale) and (c) transmittance (log scale) spectra for $\alpha = \beta = 46^\circ$, $\alpha = \beta = 44^\circ$, $\alpha = \beta = 48^\circ$, and $\alpha = 46^\circ$, $\beta = 44^\circ$.

Table 3. Bandwidth of GMR Reflector with Different Coated Thicknesses

R_0	$\alpha = 46^\circ, d_g = 326 \text{ nm}$		
	$d_L = 390 \text{ nm}$	$d_L = 400 \text{ nm}$	$d_L = 410 \text{ nm}$
$R_0 > 99\%$	$\Delta\lambda = 276 \text{ nm}$	$\Delta\lambda = 458 \text{ nm}$	$\Delta\lambda = 302 \text{ nm}$
$R_0 > 97\%$	$\Delta\lambda = 474 \text{ nm}$	$\Delta\lambda = 476 \text{ nm}$	$\Delta\lambda = 474 \text{ nm}$

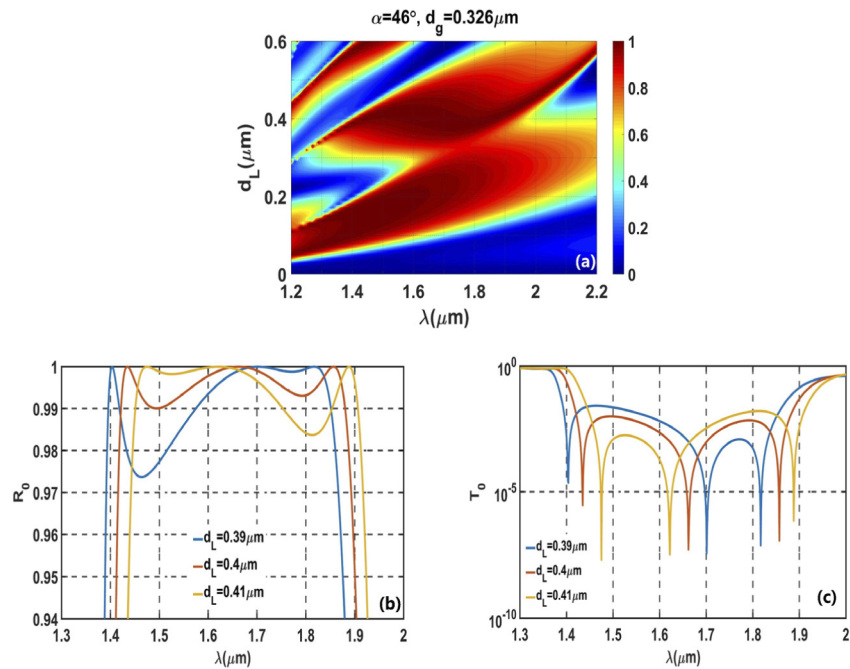


Fig. 8. (a) Contour map of zero-order reflectance in wavelength and coated layer thickness for $\Lambda = 750$ nm, $\alpha = 46^\circ$, and $d_g = 326$ nm; (b) zero-order reflectance (linear scale) and (c) transmittance (log scale) spectra for $d_L = 400, 390,$ and 410 nm.

6. Conclusions

We treated broadband GMR reflectors operating in TE polarization for normally incident light in the telecommunication spectral region. The reflectors were composed of a grating layer with triangular and trapezoidal ridge shapes on a substrate, and the high-refractive-index film layer of Si formed a conformal coverage on it. By simulating the logarithmic transmission contour map of the devices, we discovered three resonant modes in the considered range, and the interaction between them contributed to the formation of the wideband spectrum. The reflector was designed to provide a 458 nm spectral width for 99% reflectance at $\alpha = 46^\circ$, which was the best result obtained from single-period GMR reflectors with a simpler structure in TE polarization reported to date. Furthermore, it exhibited the characteristic of a broadband high reflectivity spectrum ($R > 98.4\%$ and $\Delta\lambda > 450$ nm) over a wide range of base angles from 44° to 72° . We simulated the variation in the reflection spectrum based on the equipment parameters and discovered that it exhibited different sensitivities to the grating depth, base angle, and coated layer thickness—it exhibited a higher sensitivity to the depth of the coated layer. In summary, the proposed structure provided more selectivity for the design of ultra-broadband GMR reflectors.

Funding. Fudan University-CIOMP Joint Fund (Y9S133H190); International Cooperation Project (E01142UZHO); Jilin Province Science and Technology Innovation Project of China (20190201021JC); Special fund project for high-tech industrialization of scientific and technological cooperation between Jilin Province and the Chinese Academy of Sciences (2020SYHZ0033); National Natural Science Foundation of China (NSFC) (62005273).

Disclosures. The authors declare no conflicts of interest.

Data availability. Data underlying the results presented in this paper are not publicly available at this time but may be obtained from the authors upon reasonable request.

References

1. Y. H. Ko and R. Magnusson, "Zero-contrast silicon-based metasurfaces: resonance physics and applications," *Proc. SPIE* **10356**, 103560N (2017).
2. R. Magnusson and M. Shokooh-Saremi, "Physical basis for wideband resonant reflectors," *Opt. Express* **16**(5), 3456–3462 (2008).
3. V. Lousse, W. Suh, O. Kilic, S. Kim, O. Solgaard, and S. Fan, "Angular and polarization properties of a photonic crystal slab mirror," *Opt. Express* **12**(8), 1575–1582 (2004).
4. P. Moitra, B. A. Slovick, Z. G. Yu, S. Krishnamurthy, and J. Valentine, "Experimental demonstration of a broadband all-dielectric metamaterial perfect reflector," *Appl. Phys. Lett.* **104**(17), 171102 (2014).
5. Y. H. Ko and R. Magnusson, "Wideband dielectric metamaterial reflectors: Mie scattering or leaky Bloch mode resonance?" *Optica* **5**(3), 289–294 (2018).
6. D. Rosenblatt, A. Sharon, and A. A. Friesem, "Resonant grating waveguide structures," *IEEE J. Quantum Electron.* **33**(11), 2038–2059 (1997).
7. Y. Ding and R. Magnusson, "Resonant leaky-mode spectral-band engineering and device applications," *Opt. Express* **12**(23), 5661–5674 (2004).
8. R. Magnusson, "Wideband reflectors with zero-contrast gratings," *Opt. Lett.* **39**(15), 4337–4340 (2014).
9. C. F. R. Mateus, M. C. Y. Huang, Y. Deng, A. R. Neureuther, and C. J. Chang-Hasnain, "Ultrabroadband mirror using low-index cladded subwavelength grating," *IEEE Photonics Technol. Lett.* **16**(2), 518–520 (2004).
10. S. S. Wang and R. Magnusson, "Theory and applications of guided-mode resonance filters," *Appl. Opt.* **32**(14), 2606–2613 (1993).
11. C. Chase, Y. Rao, W. Hofmann, and C. J. Chang-Hasnain, "1550 nm high contrast grating VCSEL," *Opt. Express* **18**(15), 15461–15466 (2010).
12. M. C. Y. Huang, Y. Zhou, and C. J. Chang-Hasnain, "A surface-emitting laser incorporating a high index-contrast subwavelength grating," *Nat. Photonics* **1**(2), 119–122 (2007).
13. I. I.-S. Chung, J. Mørk, P. Gilet, and A. Chelnokov, "Subwavelength Grating-Mirror VCSEL With a Thin Oxide Gap," *IEEE Photonics Technol. Lett.* **20**(2), 105–107 (2008).
14. P. Cheben, S. Janz, D.-X. Xu, B. Lamontagne, A. Delâge, and S. Tanev, "A broad-band waveguide grating coupler with a subwavelength grating mirror," *IEEE Photonics Technol. Lett.* **18**(1), 13–15 (2006).
15. R. Magnusson, M. Shokooh-Saremi, and E. G. Johnson, "Guided-mode resonant wave plates," *Opt. Lett.* **35**(14), 2472–2474 (2010).
16. C. C. Wang and S. D. Lin, "Resonant cavity-enhanced quantum-dot infrared photodetectors with sub-wavelength grating mirror," *J. Appl. Phys.* **113**(21), 213108 (2013).
17. M. Shokooh-Saremi and R. Magnusson, "Wideband leaky-mode resonance reflectors: Influence of grating profile and sublayers," *Opt. Express* **16**(22), 18249–18263 (2008).
18. I.-S. Chung, "Study on differences between high contrast grating reflectors for TM and TE polarizations and their impact on VCSEL designs," *Opt. Express* **23**(13), 16730–16739 (2015).
19. H. Wu, J. Hou, W. Mo, D. Gao, and Z. Zhou, "A multilayer-based high-performance multisubpart profile grating reflector," *IEEE Photonics Technol. Lett.* **22**(4), 203–205 (2010).
20. M. Shokooh-Saremi and R. Magnusson, "Leaky-mode resonant reflectors with extreme bandwidths," *Opt. Lett.* **35**(8), 1121–1123 (2010).
21. A. Taghizadeh, G. C. Park, J. Mork, and I. S. Chung, "Hybrid grating reflector with high reflectivity and broad bandwidth," *Opt. Express* **22**(18), 21175–21184 (2014).
22. J. Zhang, S. K. Shi, H. F. Jiao, X. C. Ji, Z. S. Wang, and A. N. D. X. B. Cheng, "Ultra-broadband reflector using double-layer subwavelength gratings," *Photonics Res.* **8**(3), 426–429 (2020).
23. S. Zhang, Y. H. Ko, and R. Magnusson, "Broadband guided-mode resonant reflectors with quasi-equilateral triangle grating profiles," *Opt. Express* **25**(23), 28451–28458 (2017).
24. G. Xing, S. Zhang, and R. Magnusson, "Leaky Bloch modal evolution of wideband reflectors with zero-contrast gratings from symmetric trapezoid to triangle ridge shapes," *Opt. Eng.* **59**(12), 127102 (2020).
25. H. Wu, L. Huang, Y. Xiao, C. Zhang, S. Li, N. Luo, X. He, and Y. Gao, "A wideband reflector realized by a subwavelength multi-subpart profile grating structure," *J. Opt.* **15**(3), 035703 (2013).
26. T. Khaleque, M. J. Uddin, and R. Magnusson, "Design and fabrication of broadband guided mode resonant reflectors in TE polarization," *Opt. Express* **22**(10), 12349–12358 (2014).
27. M. G. Moharam and T. K. Gaylord, "Rigorous coupled-wave analysis of planar-grating diffraction," *J. Opt. Soc. Am.* **71**(7), 811–818 (1981).